Accessibility of the stochastic gravitational wave background from magnetars to the interferometric gravitational wave detectors

Cheng-Jian Wu (□□□), Vuk Mandic, and Tania Regimbau

Phys. Rev. D **87**, 042002 — Published 26 February 2013

DOI: 10.1103/PhysRevD.87.042002

Accessibility of the Stochastic Gravitational Wave Background from Magnetars to the Interferometric Gravitational Wave Detectors

Chengjian Wu (吳澄劍) and Vuk Mandic
School of Physics and Astronomy, University of Minnesota, Minneapolis, MN 55455, USA

Tania Regimbau
Departement Artemis, Observatoire de la Côte d'Azur, CNRS, F-06304 Nice, France

Magnetars have been proposed as sources of gravitational waves, potentially observable by current and future terrestrial gravitational-wave detectors. In this paper, we calculate the stochastic gravitational wave background generated by summing the contributions from all magnetars in the universe and we study its accessibility to the second and third generation gravitational-wave detector networks. We perform systematic scans of the parameter space in this model, allowing the magnetic field, the ellipticity, the initial period, and the rate of magnetars to vary over the currently believed range of values. We also consider different proposed configurations of the magnetic field (poloidal, toroidal, and twisted-torus) and different proposed star-formation histories. We identify regions in the parameter space of poloidal and toroidal models that will be accessible to the second and third-generation gravitational-wave detectors, and conclude that the twisted-torus models are likely out of reach of these detectors. Poloidal field configuration with type II superconductor equation of state in the interior, or with a highly disordered magnetic field, as well as the toroidal configuration with very strong toroidal magnetic field in the interior ($> 10^{16}$ G) are the most promising in terms of gravitational-wave detection.

I. INTRODUCTION

Stochastic gravitational-wave background (SGWB) is expected to arise from the superposition of contributions from many independent and unresolved gravitational-wave (GW) sources. The SGWB could be cosmological—for example, arising in various inflationary models [1–4], or in models of cosmic (super)strings [5–9]. It could also be astrophysical, due to the superposition of waves generated by many astrophysical sources, such as compact binary coalescences [10–17] and neutron stars (quadrupole emission [18, 19] or initial instabilities [20–26], including magnetars [24, 27–30]). Magnetars, neutron stars with very strong magnetic fields, were first proposed [31] to explain the observed features of soft gamma repeaters (SGRs) and anomalous X-ray pulsars (AXPs). Besides driving the powerful electromagnetic radiation that enabled observation of these objects, the strong magnetic field is expected to induce a quadrupolar deformation in the magnetar structure, thereby generating GWs during its rapid spinning (if its symmetry axis is not aligned with the spin axis). Superposition of GWs generated by all magnetars in the universe results in a SGWB, which is the subject of this study.

Several interferometric GW detectors around the world have operated over the past decade. This includes the three LIGO detectors operating at two USA sites (Hanford, WA and Livingston Parish, LA) [32, 33], Virgo detector in Italy [34, 35], and GEO600 in Germany [36, 37]. These detectors reached their initial design sensitivities and acquired several years of data that are currently being analyzed in search for different types of GW signals. Among others, several searches for the SGWB have been completed [38–41], placing competitive upper limits on the amplitude of the SGWB.

Currently under construction is the second generation of GW detectors, including Advanced LIGO [42, 43], Advanced Virgo [44], GEO-HF [45], and KAGRA (also known as LCGT) [46]. These detectors are expected to acquire first data in 2014, with strain sensitivities about 10 times better than the initial generation of detectors. Furthermore, efforts are under way to design the third-generation GW detectors, with yet another factor of 10 in sensitivity improvement. Specifically, a design study of the Einstein Telescope project [47, 48] was completed in 2011 in Europe. While the second-generation detectors are expected to make first detections of GW signals, the third-generation detectors are expected to explore the full scientific potential of gravitational-wave astrophysics, enabling systematic studies of various GW sources, as well as probing the cosmology of the very early universe. Figure 1 shows the strain sensitivity curves for the first, the second, and the third generation of GW detectors that will be used in this study.

It has been argued that the SGWB due to magnetars may be observable by the second-generation GW detectors [24, 27–30]. In this paper we aim to precisely identify how the SGWB measurements can be used to learn about the physics that governs the behavior of magnetars, for example by constraining the equation of state in the interior of magnetars. More specifically, we perform a systematic scan of the parameter space of the magnetar SGWB model and we identify which parts of it are accessible to the second and third generation of GW detectors. We also explore three different types of the magnetic field configuration in magnetars (following [30]), as well as the importance of the uncertainty in the star formation history. In Section 2 we present the model of SGWB due to magnetars, following [29]. In Section 3 we present the

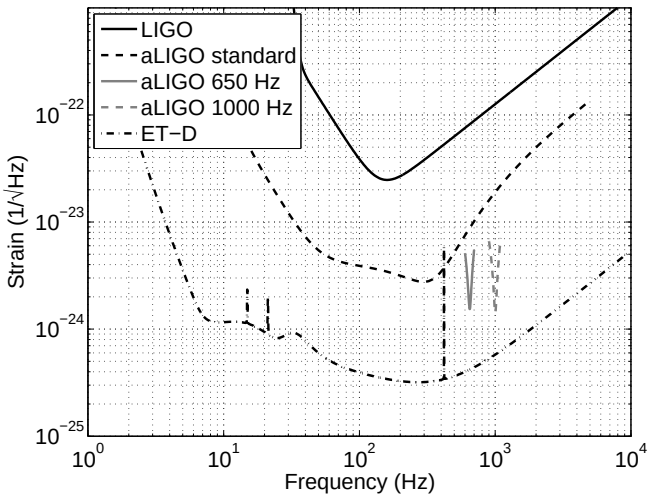

FIG. 1. Strain sensitivity curves for the initial LIGO, Advanced LIGO, and ET-D. In addition to the standard strain sensitivity, we also show the strain sensitivities for Advanced LIGO detector configurations focusing on narrow frequency bands around 650 Hz and 1 kHz. Advanced Virgo is expected to have similar strain sensitivity to that of Advanced LIGO.

results of the parameter scan, and in Section 4 we discuss the implications for the three different proposed configurations of magnetic field in magnetars. We conclude in Section 5.

II. MAGNETAR SGWB MODEL

The SGWB is usually represented in terms of the normalized GW energy spectrum [49]

$$\Omega_{\rm GW}(f) = \frac{f}{\rho_c}\frac{d\rho_{\rm GW}(f)}{df} \tag{1}$$

where $d\rho_{\rm GW}/df$ is the energy density in the frequency band $[f, f+df]$ and ρ_c is the critical energy density required to close the universe:

$$\rho_c = \frac{3H_0^2c^2}{8\pi G}, \tag{2}$$

where H_0 is the Hubble constant, c is the light speed, and G is the Newton gravitational constant. Eq. 1 can be rewritten in terms of the integrated flux density F [29]:

$$\Omega_{\rm GW}(f) = \frac{1}{\rho_c c} f F(f), \tag{3}$$

which is given by

$$F(f) = \int dP_0 p(P_0) \int_0^{z_{\rm sup}(f;P_0)} \frac{R(z)}{4\pi r^2(z)} \frac{dE_{\rm GW}}{df_e}(f_e;P_0) dz, \tag{4}$$

where $R(z)$ is the rate of magnetars as a function of redshift z, $r(z)$ is the proper distance related to the luminosity distance by $d_L(z) = (1+z)r(z)$, and dE_{GW}/df_e is the gravitational wave energy spectrum emitted by a single source at the frequency $f_e = f(1+z)$ (in the source frame), up to some maximal frequency $f_{\rm max}$. P_0 denotes the initial period of the magnetar, which determines $f_{\rm max}$. Since not all magnetars are born with the same initial period, one in principle must average over the probability distribution $p(P_0)$ of initial periods. However, assuming that magnetars are formed by the dynamo process, the range of initial periods is rather limited, $P_0 \in [1,5]$ ms [31, 50]. We can therefore approximate the integrated flux by replacing the dP_0 integral with the average value of P_0 to get

$$F(f;P_0) = \int_0^{z_{\rm sup}(f;P_0)} \frac{R(z)}{4\pi r^2(z)} \frac{dE_{\rm GW}}{df_e}(f_e;P_0) dz. \tag{5}$$

We will investigate below the importance of the choice of the P_0 value. $R(z)$ can be written in terms of the magnetar rate per unit comoving volume $R_V(z)$:

$$\begin{aligned} R(z) &= R_V(z)\frac{dV(z)}{dz} \\ &= \frac{4\pi c}{H_0}\frac{R_V(z)\, r^2(z)}{\sqrt{\Omega_M(1+z)^3+\Omega_\Lambda}} \end{aligned} \tag{6}$$

We use the standard ΛCDM cosmology, with the matter energy density $\Omega_M = 0.3$, dark energy density $\Omega_\Lambda = 0.7$ and Hubble constant $H_0 = 70$ km s^{-1} Mpc^{-1}. Finally we write the magnetar rate in terms of the star formation rate $R_*(z)$:

$$R_V(z) = \lambda \frac{R_*(z)}{1+z}. \tag{7}$$

where λ is the mass fraction per $M_\odot$ that is converted into magnetars. The $(1+z)$ term in the denominator corrects the cosmic star formation rate by the time dilatation due to the cosmic expansion.

The parameter λ captures the mass fraction $\lambda_{\rm NS}$ of neutron star progenitors (in units of $M_\odot^{-1}$) and the fraction f_m of neutron stars that are born as magnetars, $\lambda = \lambda_{\rm NS} f_m$. We will treat λ as a free parameter of this model, but we estimate its typical value here following [29]. First, assuming the Salpeter initial mass function $\xi(m)$, and assuming that the neutron star progenitors have masses larger than $8M_\odot$, and that stars with masses larger than $40M_\odot$ give rise to black holes, we have

$$\lambda_{\rm NS} = \int_{8M_\odot}^{40M_\odot} \xi(m) dm = 9\times10^{-3}\ M_\odot^{-1}. \tag{8}$$

The value of f_m is rather uncertain. Some estimates [51] and population synthesis simulations [18] suggest $f_m \approx 0.1$ but other studies suggest that all neutron stars are born as magnetars [52] (however in this case most of the magnetars will dissipate their magnetic field in a very

short time after formation). It is therefore unlikely that $\lambda > 0.01 M_\odot^{-1}$, with typical values of order $\lambda_{typical} = 10^{-3} M_\odot^{-1}$.

The cosmic star formation rate $R_*(z)$ has been studied extensively in the literature. In our calculation, we adopt the one proposed by Hopkins and Beacom [53] and set the maximum redshift $z_{\rm max} = 6$. We also repeat our calculation using four other star formation rates (SFR) and compare these five results: Fardal et al. [54], Wilkins et al. [55], Nagamine et al. [56], and Hernquist and Springel [57]. These models of star formation history are compared in Figure 2.

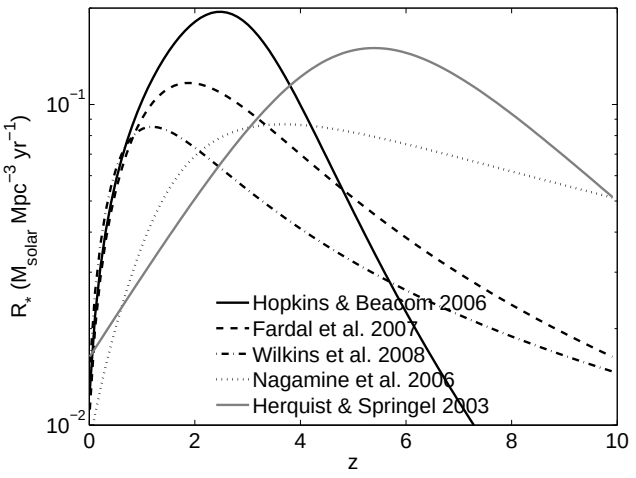

FIG. 2. Comparison of different models of star formation history: Hopkins and Beacom [53], Fardal et al. [54], Wilkins et al. [55], Nagamine et al. [56], and Hernquist and Springel [57].

We therefore rewrite Eq. 3 as

$$\Omega_{\rm GW}(f) = \frac{8\pi G}{3c^2 H_0^3}\lambda f \times \int_0^{z_{\rm sup}(f,P_0)} \frac{R_*(z)}{(1+z)\sqrt{\Omega_M(1+z)^3+\Omega_\Lambda}} \frac{dE_{\rm GW}}{df_e}(f_e;P_0)dz. \quad (9)$$

The upper limit of the integral $z_{\rm sup}$ is constrained by both $z_{\rm max}$ and $f_{\rm max}$ and is thus given by

$$z_{\rm sup}(f,P_0) = \begin{cases} z_{\rm max} & \text{if } f < \frac{f_{\rm max}(P_0)}{1+z_{\rm max}} \\ \frac{f_{\rm max}(P_0)}{f} - 1 & \text{otherwise} \end{cases}. \quad (10)$$

In other words, we exclude magnetars that produce gravitational waves with frequencies smaller than f (after redshift), as well as magnetars beyond the maximal redshift $z_{\rm max}$ of the models of star formation history we choose. We complete the model following Regimbau and Mandic [29]

$$\frac{dE_{\rm GW}}{df_e} = \frac{dE_{\rm GW}}{dt}\left|\frac{df_e}{dt}\right|^{-1} \text{ with } f_e \in [0 - 2/P_0] = I\pi^2 f_e^3 \left(\frac{5c^2R^6}{192\pi^2 G I^2}\left(\frac{\epsilon_B}{B_p}\right)^{-2} + f_e^2\right)^{-1}, \quad (11)$$

assuming that the spin axis of the neutron star is perpendicular to the magnetic axis so that gravitational waves are emitted only at twice the spinning frequency $2/P$ (with P_0 being the initial period of the star).

The spin-down rate $\frac{df_e}{dt}$ is calculated from the rate of the rotational energy loss due to electromagnetic and GW radiation [30]. The first term in the brackets of Eq. 11 comes from the electromagnetic dipole radiation, which is proportional to the magnetic field strength at the poles B_p^2. The second term is due to the GW emission. Since both $dE_{\rm GW}/dt$ and the spin-down rate due to GW emission are proportional to ϵ_B^2 [30], this term of Eq. 11 does not depend on ϵ_B^2. Overall, however, the energy spectrum $dE_{\rm GW}/df_e$ increases with $(\epsilon_B/B_p)^2$, as further discussed in Section IV.

As shown by Marassi et al. [30], if the spin and magnetic axes are not perpendicular, GWs will also be emitted at the frequency $1/P$ — in particular, the component of $\frac{dE_{GW}}{df_e}$ with $f_e = 2/P$ ($f_e = 1/P$) is proportional to $\sin^2\alpha$ ($\cos^2\alpha$) where the wobble angle α is the angle between the two axes. The precession motion will drive α towards $\pi/2$ (0) if the neutron star is prolate (oblate), and the time-scale of this process is unknown. Since the value of α and its time evolution do not significantly affect the accessibility of the GW background [30], we simplify our model to use $\alpha = \pi/2$.

We assume the neutron star radius R and the moment of inertia I to be 10 km and 10^{45} g cm^2 respectively. The magnetic field strength B_p is evaluated at the magnetic poles and is expected to be between about $10^{14} - 10^{15}$ G [58] (in this study we consider newborn magnetars and neglect a possible dissipation of the magnetic field).

The star quadrupole ellipticity ϵ_B is determined by the magnetic field configuration and strength. However, we will first study the model assuming no relationship between the ellipticity and the magnetic field, and will then consider three specific magnetic field configurations (poloidal, toroidal, and twisted torus) which will imply different relations between the magnetic field strength and ellipticity.

The continuity of the GW signal produced by the magnetars is characterized by its duty cycle D. Assuming $\tau(z)$ is the average signal duration of magnetars at redshift z, the duty cycle is defined by

$$D = \int_0^{z_{\rm sup}} R(z)\tau(z)(1+z)dz, \quad (12)$$

where $1+z$ rescales $\tau(z)$ to account for the time-dilation effect. By summing up the time duration of all magnetars, Marassi et al. [30] showed that the duty cycle of the SGWB from magnetar population $D \gg 1$, confirming that the produced background is continuous in time.

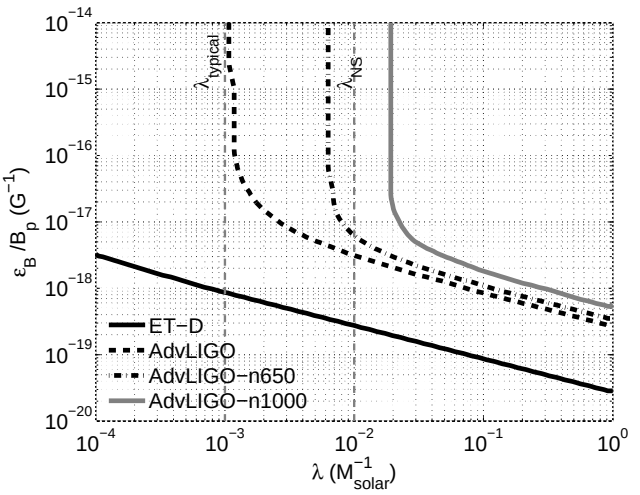

FIG. 3. We show regions of the parameter space of the magnetar SGWB model accessible to the future second-generation detectors (Advanced LIGO [42, 43]) and third-generation detectors (Einstein Telescope [47, 48]). The accessible regions are above the corresponding curves. We assume star formation rate from [53] and the initial period $P_0 = 1$ ms.

III. ACCESSIBILITY TO THE SECOND AND THIRD GENERATION DETECTORS

We scan the parameter space of the magnetar SGWB model described in Section II. In particular, since the spectrum depends on the ratio of ellipticity and the polar magnetic field, we will treat ϵ_B/B_p as one free parameter, ranging between 10^{-20} and 10^{-14} G^{-1}. We will also treat λ as a free parameter, allowing it to take values in the range $10^{-4} - 1$ M$_\odot^{-1}$, although the likely value of this parameter is expected to be $\lambda < 10^{-2}$ M$_\odot^{-1}$. We therefore scan the $\epsilon_B/B_p - \lambda$ plane, and for each point in this plane we compute $\Omega_{\rm GW}(f)$. We then compare the spectrum to the projected sensitivities for the second and third-generation GW detectors. For the second generation, we assume the standard Advanced LIGO expected strain sensitivity [42, 43], and also explore the detector configurations where the strain sensitivity is amplified at 650 Hz or 1 kHz. For the third generation, we assume the ET-D strain sensitivity curve of Einstein Telescope [47, 48]. In all cases, the projected sensitivity is defined as the signal-to-noise ratio of 2, assuming two co-located detectors and one year of exposure.

The results of the scan are shown in Figure 3 using the star formation rate from [53] and $P_0 = 1$ ms. The second-generation detectors will be able to probe large parts of this parameter space, reaching even the typical values of the magnetar rate, $\lambda \sim 10^{-3}$ M$_\odot^{-1}$. Some parts of the parameter space, corresponding to $\lambda \gtrsim 10^{-2}$ M$_\odot^{-1}$ and $\epsilon_B/B_p \gtrsim 10^{-17}$ G^{-1}, may be accessible to multiple frequency bands of the second-generation detectors, allowing a more detailed study of the SGWB spectrum. The vertical part of the LIGO and Advanced LIGO curves, where the spectrum is not sensitive to ϵ_B/B_p, corresponds to the regime where GW emission dominates over the electromagnetic emission - in this case, the second term in the bracket of Eq. 11 dominates over the first one, so the whole bracket can be approximated at f_e^{-2}, independent of ϵ_B/B_p. The third-generation detectors will be able to probe a substantially larger part of this parameter space, reaching much lower values of the magnetar rate and ϵ_B/B_p.

To estimate the importance of the choice of the star formation rate model and of the initial period P_0, we computed the sensitivity curves for the second and third-generation detectors using five different models of star formation rate [53–57] and five different values of P_0. The results are shown in Figure 4—the uncertainties in the star formation rate and in the initial period lead to a factor of 3-4 uncertainty in the ϵ_B/B_p parameter.

IV. IMPLICATIONS

We now investigate the implications of the results of our scans for different magnetic field configurations of magnetars. Since different field configurations imply different relations between the magnetic field and the ellipticity of the magnetar, the SGWB searches can be used to probe these different field configurations and the physics that gives rise to them. In general, a poloidal magnetic field extends throughout both the interior and the exterior of the magnetar with the expected field strength of $B_p \sim 10^{14} - 10^{15}$ G [58]. In addition, a toroidal magnetic field component has been suggested to exist within a torus-shaped region inside the magnetar [27, 59, 60] in order to account for the observed features of the soft gamma repeaters (SGRs) and the anomalous X-ray pulsars (AXPs). Following Marassi et al. [30] we consider three different cases: poloidal-dominated, toroidal-dominated, and twisted-torus configurations. For each case we assume the star formation rate from Hopkins & Beacom [53] and $P_0 = 1$ ms.

A. Poloidal-Dominated Field Configuration

In the poloidal magnetic field configuration, the ellipticity is given by

$$\epsilon_B = \beta \frac{R^8 B_p^2}{4GI^2}, \tag{13}$$

following Bonazzola and Gourgoulhon [61]. The distortion parameter β is dimensionless and it accounts for the magnetic field geometry and the equation of state (EOS). Numerical simulations [61] indicate that if the interior of the neutron star is a normal conductor, the distortion parameter is typically $\beta < 10$, even if the current flow is limited to the core of the star. If the star's interior is a type I superconductor, such that the magnetic

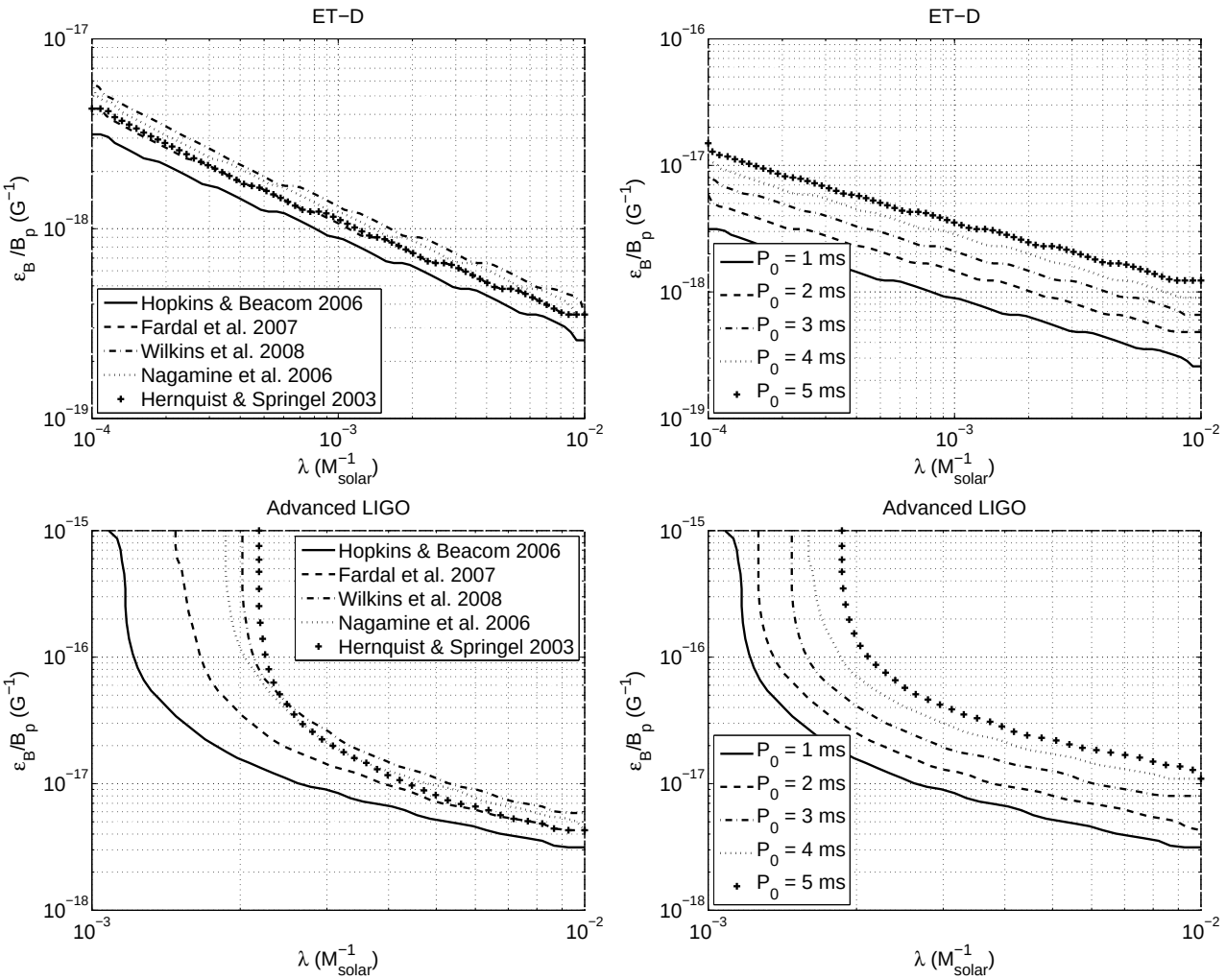

FIG. 4. Top-left: Comparison of the third-generation sensitivity curves (ET-D) for $P_0 = 1$ ms and for five different choices of star formation rate [53–57]. Top-right: Comparison of the third-generation sensitivity curves (ET-D) for the Hopkins and Beacom star formation rate model [53] and for five different values of P_0. Bottom-left: same as top-left but for the second-generation detectors (standard Advanced LIGO strain sensitivity). Bottom-right: same as top-right, but for the second-generation detectors (standard Advanced LIGO strain sensitivity).

field is expelled from parts of the star, the distortion parameter could be significantly larger, reaching values of several hundred. Even larger distortions are expected in the case of the highly disordered (stochastic) magnetic field in the interior - in such cases the overall (average) magnetic dipole moment could be very small, but the distortion parameter can reach values $\beta > 1000$. Similarly, in the case of type II superconducting interior, very large stresses in the crust of the star could also lead to values of $\beta > 1000$. It is therefore possible to turn the SGWB constraints on ϵ_B into constraints on β, hence extracting information about the equation of state in magnetars, in the framework of poloidal-dominated magnetic field configuration.

In Figure 5 we show the sensitivity curves for the second and third-generation detectors in the $\beta - \lambda$ plane, for several values of B_p in the range $10^{14} - 10^{16}$ G. As noted above, the second-generation detectors will be able to probe only models where the magnetar rate is relatively large, larger than the "typical" value of $10^{-3}\ \mathrm{M}_\odot^{-1}$. Depending on the average strength of the poloidal magnetic field, these detectors will probe models with largest values of β, corresponding to the type II superconductor or to highly disordered (stochastic) magnetic field in the interior of the star. They may also be able to probe some of the type-I superconductor models. The non-superconductor models will be out of reach of the second-generation detectors. The third-generation detectors will be able to explore a significantly larger part of this parameters space, potentially exploring the entire type-I and type-II superconductor regions down to rather low magnetar rates of $\lambda \sim 10^{-4}\ \mathrm{M}_\odot^{-1}$ (for largest values of B_p). These detectors may even be able to probe the non-superconductor equation of state for the largest

values of B_p and λ.

B. Twisted-Torus Magnetic Field Configuration

The twisted-torus magnetic field configuration was introduced by Braithwaite & Spruit [59]. It is argued to be a universal equilibrium structure of the magnetic field [62], while the pure poloidal field configuration is potentially unstable [63]. The twisted-torus field configuration takes a toroidal magnetic field closed in the interior of the magnetar into account. The toroidal field is twisted and stabilizes the poloidal field. The resulting ellipticity can be modelled by

$$\epsilon_B = k \left(\frac{B_p}{10^{15} G} \right)^2 \times 10^{-6}, \tag{14}$$

where k is a dimensionless parameter dependent on the field geometry and the equation of state. Ciolfi et al. [64] argue that for the twisted-torus field configuration $k = 4 - 9$ spans a realistic range of the star compactness at $B_p = 1 \times 10^{16}$ G in the framework of general relativity. More specifically, $k = 4$ corresponds to a small compactness given by the Akmal-Pandharipande-Revenhall equation of state [65], and $k = 9$ corresponds to a large compactness given by the Glendenning equation of state [66].

The Figure 6 shows the sensitivity curves of the second and third-generation detectors in the $k - B_p$ plane for several values of λ. The realistic range of k values is far below the sensitivities of both detector generations, implying that the twisted-torus field configuration models will not be reachable by these detectors.

C. Toroidal-dominated field configuration

Very strong toroidal magnetic field component, $B_t \gtrsim 10^{16}$ G, has been proposed for the interior of the magnetar to explain the enormous energy emission in the December 27, 2004 giant flare from the SGR 1806-20, as argued by Stella, Dall'Osso and Israel [60]. Braithwaite further investigated the stability of the relative strengths of the toroidal and poloidal components, confirming that a magnetar can indeed have such a toroidal-dominated field configuration [67]. To model the ellipticity, we adopt the estimate by Cutler [27]:

$$\epsilon_B = \begin{cases} -1.6 \times 10^{-6} (B_t / 10^{15} G), & B_t < 10^{15} \mathrm{G} \\ -1.6 \times 10^{-6} (B_t / 10^{15} G)^2, & B_t > 10^{15} \mathrm{G} \end{cases} . \tag{15}$$

In the framework of the toroidal-dominated models, it is therefore natural to study the GW detector sensitivities in the $B_t - B_p$ plane, as shown in Figure 7. While the second-generation detectors will be able to probe only models with relatively strong toroidal field component (reaching $B_t \sim 10^{16}$ G only for the largest magnetar rate values λ, and $B_t \sim 10^{17}$ G for the more typical $\lambda \sim 10^{-3}\,\mathrm{M}_\odot^{-1}$), the third-generation detectors will be able to probe much of the interesting parameter space in these models.

V. CONCLUSION

In this paper we conducted a systematic study of the parameter space in the model of stochastic gravitational-wave background due to magnetars, and we identified the regions of this parameter space that will be probed by the upcoming second and third-generation gravitational wave detectors. We first computed these regions for the general case, without assuming a specific magnetic field configuration in the magnetars, in the plane spanned by two critical parameters: the ratio of ellipticity and the polar magnetic field, ϵ_B / B_p, and the rate of magnetars λ. We found that different choices of the star formation history and of the initial period of magnetars P_0 lead to a factor of 3-4 uncertainty in the computed accessible regions of this parameter space. Similar level of uncertainty is also expected due to the uncertainty in the assumed values of the average neutron star radius ($R \approx 10$ km) and the moment of inertia ($I \approx 10^{45}$ g cm^2).

We then proceeded to apply our results to three different magnetic field configurations proposed in the literature, which imply different relations between the magnetar ellipticity and its magnetic field strength. We found that the twisted-torus field configuration models will not be reachable by either the second or the third generation of gravitational wave detectors. In the case of poloidal-dominated configuration, the second-generation detectors will be able to probe models with largest distortions in the shape of the magnetar, corresponding to the type-II superconductor equation of state or the highly-disordered magnetic field in the interior, for magnetar rates larger than "typical", $\lambda > 10^{-3}\,\mathrm{M}_\odot^{-1}$. The third-generation detectors will be able to also probe models with type-I superconductor equation of state, even for very low magnetar rates $\lambda \sim 10^{-4}\,\mathrm{M}_\odot^{-1}$. The toroidal-dominated magnetic field configuration models will be probed by both second and third-generation detectors—the third-generation detectors will be able to explore a large fraction of the interesting parameter space in these models, reaching relatively low values of the toroidal magnetic field strength $B_t \sim 10^{16}$ G.

The work of CW and VM was in part supported by the NSF grant PHY0758036.

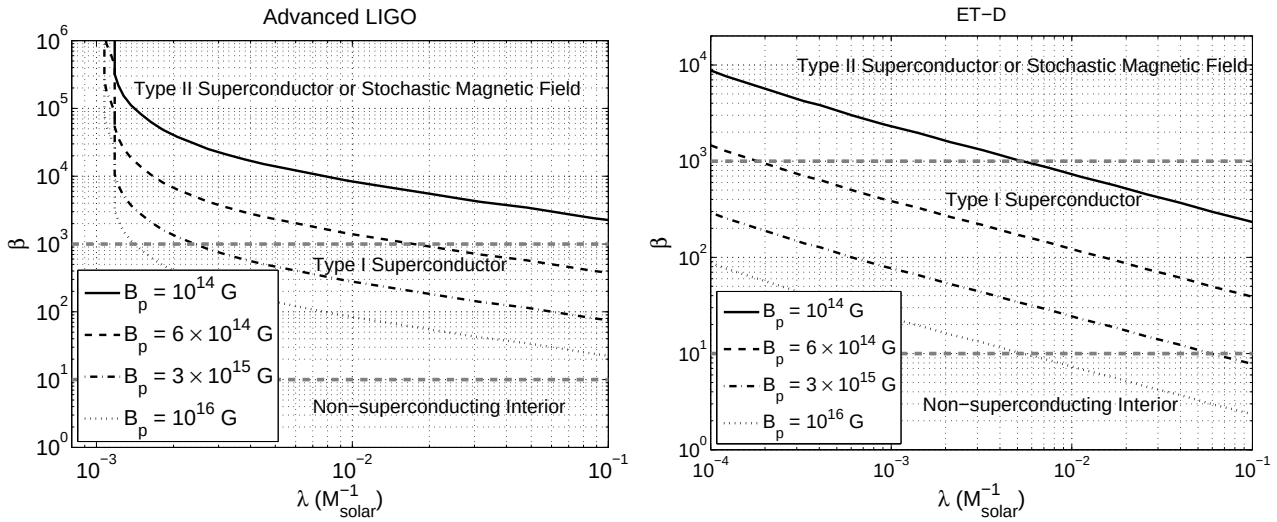

FIG. 5. Sensitivity curves in the $\beta - \lambda$ plane for the poloidal magnetic field configuration with different values of B_p are shown for the second (left) and third (right) generation of GW detectors. We use the star formation rate from Hopkins and Beacom [53] and $P_0 = 1$ ms. The gray horizontal dashed lines denote different types of the equation of state in the interior of magnetars, in the framework of a pure poloidal field configuration.

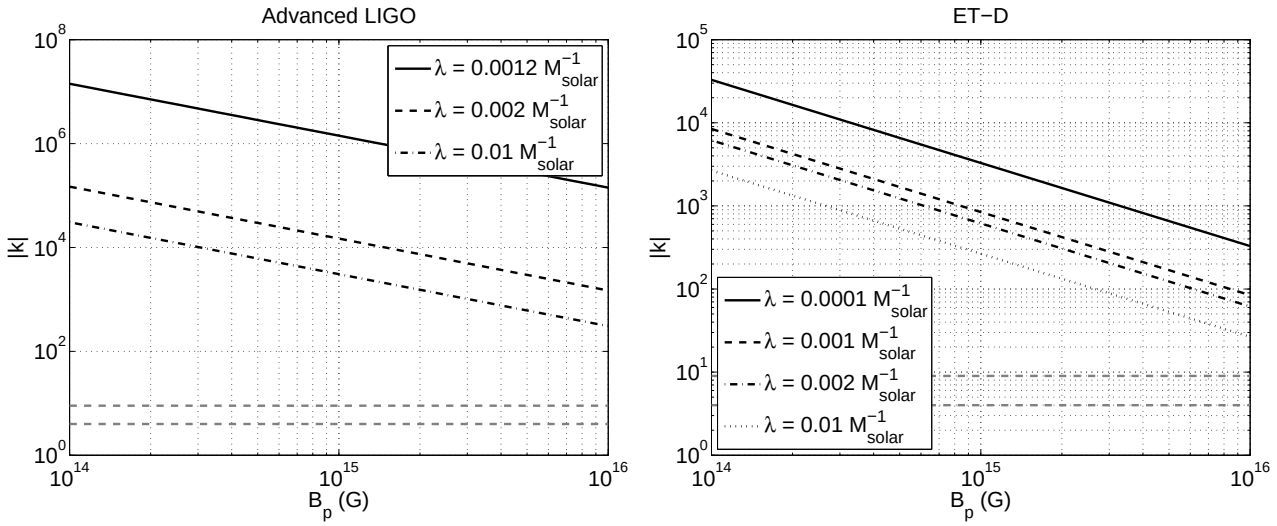

FIG. 6. Sensitivity curves in the $k - B_p$ plane of the twisted-torus field configuration models are shown for several values of λ for the second (left) and third (right) generation of gravitational-wave detectors. We assume star formation rate model from Hopkins and Beacom [53] and $P_0 = 1$ ms. The two gray horizontal dashed lines denote the realistic range of values for k [64].

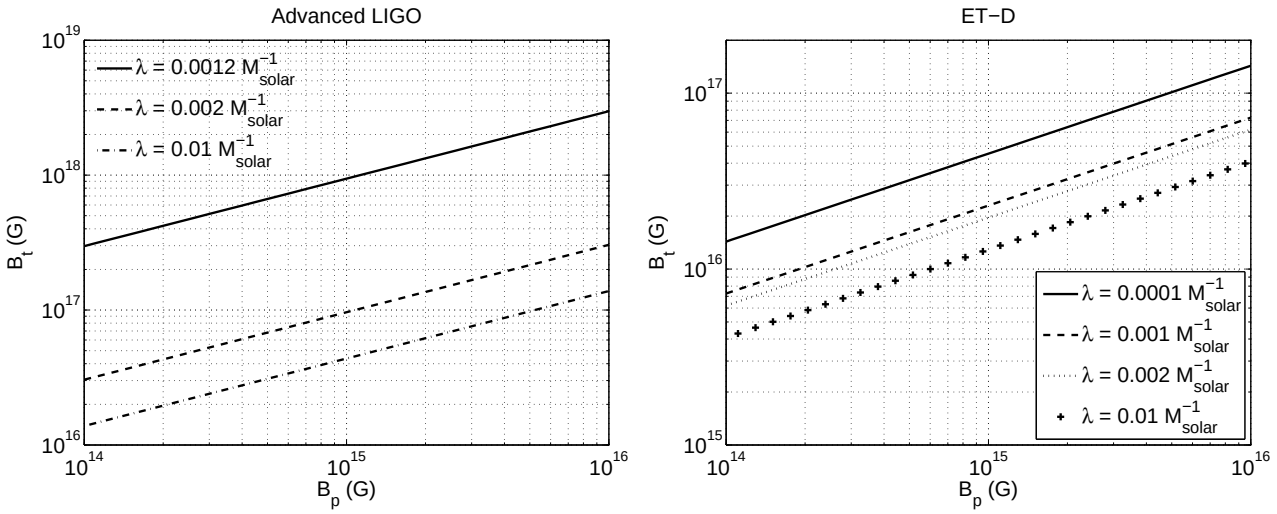

FIG. 7. Sensitivity curves in the $B_t - B_p$ plane of toroidal-dominated field configuration models are shown for different values of λ, for the second (left) and third (right) generation of gravitational-wave detectors. We assume the star formation rate from Hopkins and Beacom [53] and $P_0 = 1$ ms.

[1] L. P. Grishchuk, Sov. Phys. JETP **40**, 409 (1975).
[2] A. A. Starobinskii, JETP Lett. **30**, 682 (1979).
[3] R. Easther and E. A. Lim, JCAP **0604**, 010 (2006).
[4] N. Barnaby, E. Pajer, and M. Peloso, arXiv:1110.3327 (2011).
[5] R. R. Caldwell and B. Allen, Phys. Rev. D **45**, 3447 (1992).
[6] T. Damour and A. Vilenkin, Phys. Rev. Lett. **85**, 3761 (2000).
[7] T. Damour and A. Vilenkin, Phys. Rev. D **71**, 063510 (2005).
[8] X. Siemens, V. Mandic, and J. Creighton, Phys. Rev. Lett. **98**, 111101 (2007).
[9] S. Olmez, V. Mandic, and X. Siemens, Phys. Rev. D **81**, 104028 (2010).
[10] E. S. Phinney, Astrophys. J. Lett. **380**, L17 (1991).
[11] D. I. Kosenko and K. A. Postnov, Astron. & Astrop. **336**, 786 (1998).
[12] T. Regimbau, Res. Astr. Astrop. **11**, 369 (2011).
[13] T. Regimbau and J. de Freitas Pacheco, Astrop. J. **642**, 455 (2006).
[14] X.-J. Zhu, E. Howell, T. Regimbau, D. Blair, and Z.-H. Zhu, Astrophys. J. **739**, 86 (2011).
[15] P. A. Rosado, Phys. Rev. D **84**, 084004 (2011).
[16] S. Marassi, R. Schneider, G. Corvino, V. Ferrari, and S. P. Zwart, Phys. Rev. D **84**, 124037 (2011).
[17] C. Wu, V. Mandic, and T. Regimbau, Phys. Rev. D **85**, 104024 (2012).
[18] T. Regimbau and J. A. de Freitas Pacheco, Astron. and Astrophys. **376**, 381 (2001).
[19] P. Rosado, arXiv:1206.1330 (2012).
[20] B. J. Owen, L. Lindblom, C. Cutler, B. F. Schutz, A. Vecchio, and N. Andersson, Phys. Rev. D **58**, 084020 (1998).
[21] S. Chandrasekhar, *"Ellipsoidal Figures of Equilibrium"* (New Haven, Yale Univ. Press, 1969).
[22] J. L. Houser, J. M. Centrella, and S. C. Smith, Phys. Rev. Lett. **72**, 1314 (1994).
[23] D. Lai and S. L. Shapiro, Astrophys. J. **442**, 259 (1995).
[24] E. Howell *et al.*, Mon. Not. Roy. Astro. Soc. **410**, 2123 (2011).
[25] X. Zhu *et al.*, Astrophys. J. **729**, 59 (2011).
[26] V. Ferrari *et al.*, Mon. Not. Roy. Astro. Soc. **303**, 258 (1999).
[27] C. Cutler, Phys. Rev. D **66**, 084025 (2002).
[28] T. Regimbau and J. de Freitas Pacheco, Astron. Astrop. **447**, 1 (2006).
[29] T. Regimbau and V. Mandic, Class. Quant. Grav. **25**, 184018 (2008).
[30] S. Marassi, R. Ciolfi, R. Schneider, L. Stella, and V. Ferrari, Mon. Not. Roy. Astron. Soc. **411**, 2549 (2010).
[31] R. Duncan and C. Thompson, Astrop. J. Lett. **392**, 9 (1992).
[32] B. Abbott *et al.*, Nucl. Instr. Meth. A **517**, 154 (2004).
[33] B. Abbott *et al.*, Rep. Prog. Physs **72**, 076901 (2009).
[34] F. Acernese *et al.*, Class. Quant. Grav. **25**, 184001 (2008).
[35] T. Accadia *et al.*, Class. Quant. Grav. **28**, 114002 (2011).
[36] B. Willke *et al.*, Class. Quant. Grav. **21**, S417 (2004).
[37] H. Grote *et al.*, Classical Quantum Gravity **27**, 084003 (2010).
[38] B. Abbott *et al.*, Phys. Rev. Lett. **95**, 221101 (2005).
[39] B. Abbott *et al.*, Astrop. J. **659**, 918 (2007).
[40] B. Abbott *et al.*, Nature **460**, 990 (2009).
[41] J. Abadie *et al.*, Phys. Rev. D **85**, 122001 (2012).
[42] T. A. LIGO Team, Internal working note of the LIGO Laboratory LIGO-M060056-10-M (2007).
[43] G. Harry, Class. Quant. Grav. **27**, 084006 (2010).
[44] T. V. Collaboration", Advanced Virgo Conceptual Design Virgo Report VIR 042A 07 (2007).
[45] B. Willke *et al.*, Class. Quant. Grav. **23**, S207 (2006).
[46] K. Kuroda, Class. Quant. Grav. **27**, 084004 (2010).
[47] T. E. science team, https://tds.ego-gw.it/ql/?c=7954 (2011).
[48] M. Punturo *et al.*, Class. Quant. Grav. **27**, 084007 (2010).
[49] B. Allen and J. D. Romano, Phys. Rev. D **59**, 102001 (1999).
[50] C. Thompson and R. Duncan, Astrop. J. **403**, 194 (1993).
[51] C. Kouveliotou *et al.*, Nature **393**, 235 (1998).
[52] R. Heras, arXiv:1104.5060 (2011).
[53] A. Hopkins and J. Beacom, Astrop. J. **651**, 142 (2006).
[54] M. Fardal, N. Katz, D. Weinberg, and R. Davé, Mon. Not. Roy. Astron. Soc. **379**, 985 (2007).
[55] S. Wilkins, N. Trentham, and A. Hopkins, arXiv:0803.4024 (2008).
[56] K. Nagamine, J. Ostriker, M. Fukugita, and R. Cen, Astrop. J. **653**, 881 (2006).
[57] L. Hernquist and V. Springel, Mon. Not. Roy. Astron. Soc. **341**, 1253 (2003).
[58] C. Thompson and R. Duncan, Astrop. J. **473**, 322 (1996).
[59] J. Braithwaite and H. Spruit, Nature **431**, 819 (2004).
[60] L. Stella, S. Dall'Osso, G. Israel, and A. Vecchio, Astrop. J. **634**, L165 (2005).
[61] S. Bonazzola and E. Gourgoulhon, Astron. Astrop. **312**, 675 (1996).
[62] S. Yoshida, S. Yoshida, and Y. Eriguchi, Astrop. J. **651**, 462 (2006).
[63] S. Lander and D. Jones, Mon. Not. Roy. Astron. Soc. **412**, 1730 (2010).
[64] R. Ciolfi, V. Ferrari, and L. Gualtieri, Mon. Not. Roy. Astron. Soc. **406**, 2540 (2010).
[65] A. Akmal, V. R. Pandharipande, and D. G. Ravenhall, Phys. Rev. C **58**, 1804 (1998).
[66] N. Glendenning, Astrop. J. **293**, 470 (1985).
[67] J. Braithwaite, Mon. Not. Roy. Astron. Soc. **397**, 763 (2009).